Solar Energy Materials & Solar Cells 144 (2016) 165–172

Contents lists available at ScienceDirect

Solar Energy Materials & Solar Cells

journal homepage: www.elsevier.com/locate/solmat

Blue colloidal nanoparticles of molybdenum oxide by simple anodizing method: decolorization by $PdCl_2$ and observation of in-liquid gasochromic coloration

F. Delalat, M. Ranjbar*, H. Salamati

Department of Physics, Isfahan University of Technology, Isfahan, 84156-83111, Iran

ARTICLE INFO

Article history:
Received 27 June 2015
Received in revised form
29 August 2015
Accepted 31 August 2015

Keywords:
Blue molybdenum oxide
Nanoparticles
Anodizing
Decolorization
$PdCl_2$
Gasochromic
XPS

ABSTRACT

In this study, colloidal nanoparticles of molybdenum oxide were prepared through a simple electrochemical anodizing of molybdenum sheets in 0.02 M HCl electrolyte. The initial transparent electrolyte turned into a long-term stable dark blue color during the anodizing process. The blue liquid exhibited several optical absorption peaks and shoulders at photon energies of 1.2, 1.4, 1.6 and 1.9 eV. However, to examine the gasochromic coloration in the liquid phase, the colloidal solution must be initially colorless. Moreover, the liquid with gasochromic property is required to be catalytically active against hydrogen gas. These tasks were performed by adding precursor $PdCl_2$ solution. It was observed that $PdCl_2$ not only activates the liquid for gasochromic coloration, but also removes the initial blue color. General characterizations were performed on drop-dried samples by means of transmission electron microscopy (TEM), UV–vis spectroscopy and X-ray photoelectron spectroscopy (XPS). The decolorized colloidal molybdenum oxide samples exhibited unique in-liquid gasochromic colorations by diluted hydrogen bubbling, which converted the colorless solutions back to the dark blue color. The gasochromically colored samples showed absorption bands analogous to those of as-prepared blue samples along with an extra shoulder at around 3 eV. The coloration mechanism was described according to two existing models; small polaron and charge transfer models.

1. Introduction

Gasochromic coatings and glazing of transition metal oxides have been investigated for several decades [1–4]. In the gasochromic phenomenon, an electrochromic film such as tungsten oxide covered with a thin Pd or Pt layer (4–5 nm thickness) is able to switch from a bleach or transparent state to a dark blue absorbing state when they are exposed to hydrogen gas. Meanwhile, the color switching can occur between transparent and mirror states too, which have been observed for thin films of certain metal hydrates such as MgNi alloys [5,6]. For each kind, this process is often reversible; when H_2 is replaced with O_2, the colored state reversibly turns to bleach. Gasochromic coating have been used for different applications such as optical hydrogen gas sensing, hydrogen leak detecting, smart mirrors and windows [7–9].

Up to now, the main objectives have focused on thin films of gasochromic materials and little has been done on new systems like colloidal solutions. Moreover, gasochromic thin films often exhibit a single broad absorption peak in NIR when they are colored [10–14]. This broad peak is unable to entirely interpret the chromic phenomena in details and must be de-convoluted manually into some constructing narrower peaks. Moreover, hydrogen transfer into the lattice as the first step of gasochromic coloration is limited in a rigid thin solid film due to one dimensional diffusion across the layer. Nevertheless, colloidal nanoparticles provide greater diffusion constants for a gas as they are dispersed in a fluid and absorb incoming hydrogen faster as they have great surface to volume ratio. In the gasochromic system, the hydrogen catalyst (Pd or Pt) plays critical role because it controls hydrogen dissociation rate under the spill-over mechanism [15,16]. One more advantage of colloidal systems is that the adding of the salt solution of the noble metals Pd and Pt into the gasochromic colloids creates the activation against hydrogen gas simply. Studying on tungsten oxide colloidal nanoparticles prepared by laser ablation [17] or anodizing [18] in the liquid and activated by palladium chloride, we have recently demonstrated that colloidal forms of gasochromic materials have the capability of in-liquid gasochromic coloration with unique optical properties demonstrating distinct optical absorption bands instead of one NIR region broad peak. Up to now, the most studied material for gasochromic is

* Corresponding author. Tel.: +98 31 3391 2375; fax: +98 313 391 2376.
E-mail address: ranjbar@cc.iut.ac.ir (M. Ranjbar).

http://dx.doi.org/10.1016/j.solmat.2015.08.038
0927-0248/

tungsten oxide films with a variety of texture, morphology and composition, which have shown fast coloring, durability and good reversibility. However, molybdenum oxide is one another material with great ability of gasochromic coloration and has been known as a good photochromic material. Few reports on gasochromic coloration of molybdenum oxide thin films exist in literature [19–21] and most of which has not shown coloring reversibility. Additionally, to the best of our knowledge, no report on in-liquid gasochromic coloration of a colloidal molybdenum oxide has emerged up to now. For that reason, it is of scientific and technical benefit to explore the gasochromic coloration of the colloidal solutions of molybdenum oxide. Meanwhile molybdenum oxide has recently attracted much attentions for its applications in gas sensing [22,23], field emission [24] cathode of batteries [25,26] electrochromic [27] and photochromic [28].

Until now, different methods have been used for production of molybdenum oxide nanoparticles including liquid exfoliation [29], plasma processing [30], soft chemical process [31] and water bath method [32]. In our previous work on tungsten oxide based gasochromic liquid, we have used a simple anodizing method for synthesis of gasochromic tungsten oxide colloids. In the electrochemical anodizing process, the metallic anode is oxidized to a metal oxide, fragmented into very small pieces, is dispersed into the electrolyte and gives a homogenous colloidal solution. It is noteworthy that hydrate forms of metal oxides, which have been obtained by anodizing method, are good candidates owing to their property of high proton transportation. The method of anodizing has been also used in a few papers for synthesis of metal oxides of other elements such as titanium compounds [33,34]. Although people are familiar with this process in electrochemistry or corrosion science, less attention has been paid to it as a method for generation of colloidal solutions and nanoparticles. In the present work, this idea is extended to molybdenum oxide for synthesis of nanoparticles via the anodizing of Mo sheets in an acidic electrolyte and their gasochromic properties in the liquid phase are investigated. Besides, colloidal nanoparticles dispersed in a liquid often exhibit different chromic performance comparing with bulk or thin films types. In the case of molybdenum oxide, for example, the photochromic performance has been observed to be different from molybdenum oxide thin films [35]. This is due to the particles that are separated from each other in solutions and accordingly much effective surface area is available to expose to incoming light. In addition, colloids in nanoscale often present extra absorption bands in optical spectra. This assists better understanding the underlying physical mechanisms. In the work on tungsten oxide, anodizing of tungsten rods in acidic electrolyte led to formation of tungsten oxide dehydrate colloids which were initially transparent (colorless). In this study, however, anodizing of molybdenum led to formation of molybdenum oxide colloids with a dark blue color.

Since gasochromic investigations need primarily colorless samples therefore we had to remove the initial blue color. Accordingly, this will be an important point to be addressed in this paper. We found that addition of palladium salt ($PdCl_2$) solution, which is used in our method as the source of hydrogen catalyst, also leads to gradually decolorization of the as-prepared blue colloidal molybdenum oxide solutions with a salt concentration-dependent decolorization rate. Under hydrogen gas exposure, this composition of colorless colloidal solution was able to be converted nearly to its initial blue color along with an extra shoulder at around 3 eV. The variations of optical absorption in the bleaching process of gasochromically colored samples were interpreted by the small polaron and inter-band transition models. Here, TEM, XPS, and UV–vis spectrophotometer tools were used for characterization of produced nanoparticles. Fig. 1 indicates the process from anodizing to in-liquid gasochromic coloration.

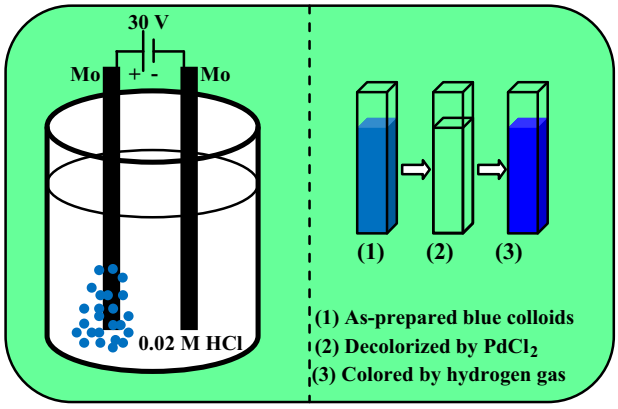

Fig. 1. Schematic representation of synthesis of molybdenum oxide nanosheets by anodizing method, as-prepared blue colloids, decolorization and activation against hydrogen gas by $PdCl_2$ and gasochromic coloring by hydrogen bubbling. (For interpretation of the references to color in this figure legend, the reader is referred to the web version of this article.)

2. Experimental

Colloidal nanoparticles of molybdenum oxide were fabricated via an electrochemical anodizing of molybdenum sheets in a 0.02 M HCl electrolyte. In this process, two molybdenum sheets were put 1 cm apart from each other into a 0.02 M HCl electrolyte. A 30 V DC bias voltage was applied to the two ends of sheets for 5 min (Fig. 1). By applying voltage, the anode began to corrode electrochemically, gradually dispersed throughout the electrolyte and the colloidal solution were obtained. Total dispersion of molybdenum were measured from the weight loss of molybdenum sheets. $PdCl_2$ solution was prepared by adding 0.02 g of $PdCl_2$ powder (99.99% purity) into a mixture of 99.9 cc DI water and 0.1 cc HCl. This composition was kept in ultrasonic bath for 3 h until $PdCl_2$ powder was dissolved entirely and a uniform yellowish solution of 0.2 g/l $PdCl_2$ was obtained. Then, by addition of $PdCl_2$ solution to the colloidal molybdenum oxide, samples of different Pd:Mo ratios (1:20, 1:15, 1:10 and 1:5) were obtained. They were named according to the Pd:Mo ratio (for example $PM_{1:10}$ denotes Pd:Mo = 1:10). In order to perform some characterizations, the certain samples were prepared by drop-drying of colloidal solution onto quartz substrates or TEM girds. TEM imaging was performed using Philips Holland model CM120. The XPS analyses were done using an ESCA/AES system. The ESCA system was equipped with a concentric hemispherical analyzer (CHA, Specs model EA10 plus) suitable for Auger electron spectroscopy and XPS. For exciting the X-ray photoelectrons, an AlKα line at 1486.6 eV was used. The energy scale was calibrated against the carbon binding energy (284.8 eV). Optical absorptions were measured in the 190–1100 nm wavelength range using Perkin Elmer spectrophotometer (Lambda 25). Gasochromic investigations were performed using (10%H_2)/Ar mixed gas for coloring and O_2 (purity 99.9%) for bleaching which were alternatively bubbled into the $PM_{1:15}$ colloidal solutions through a tiny glass pipe.

3. Results and discussion

3.1. TEM

Fig. 2(a) shows a typical TEM image and corresponding size distribution histogram of as-prepared sample. Crystallites of polygon-shape are observable in the TEM image that resembles nanosheets in some part of image. In the inset, for example, nanoparticles are placed over each other in such a way so that

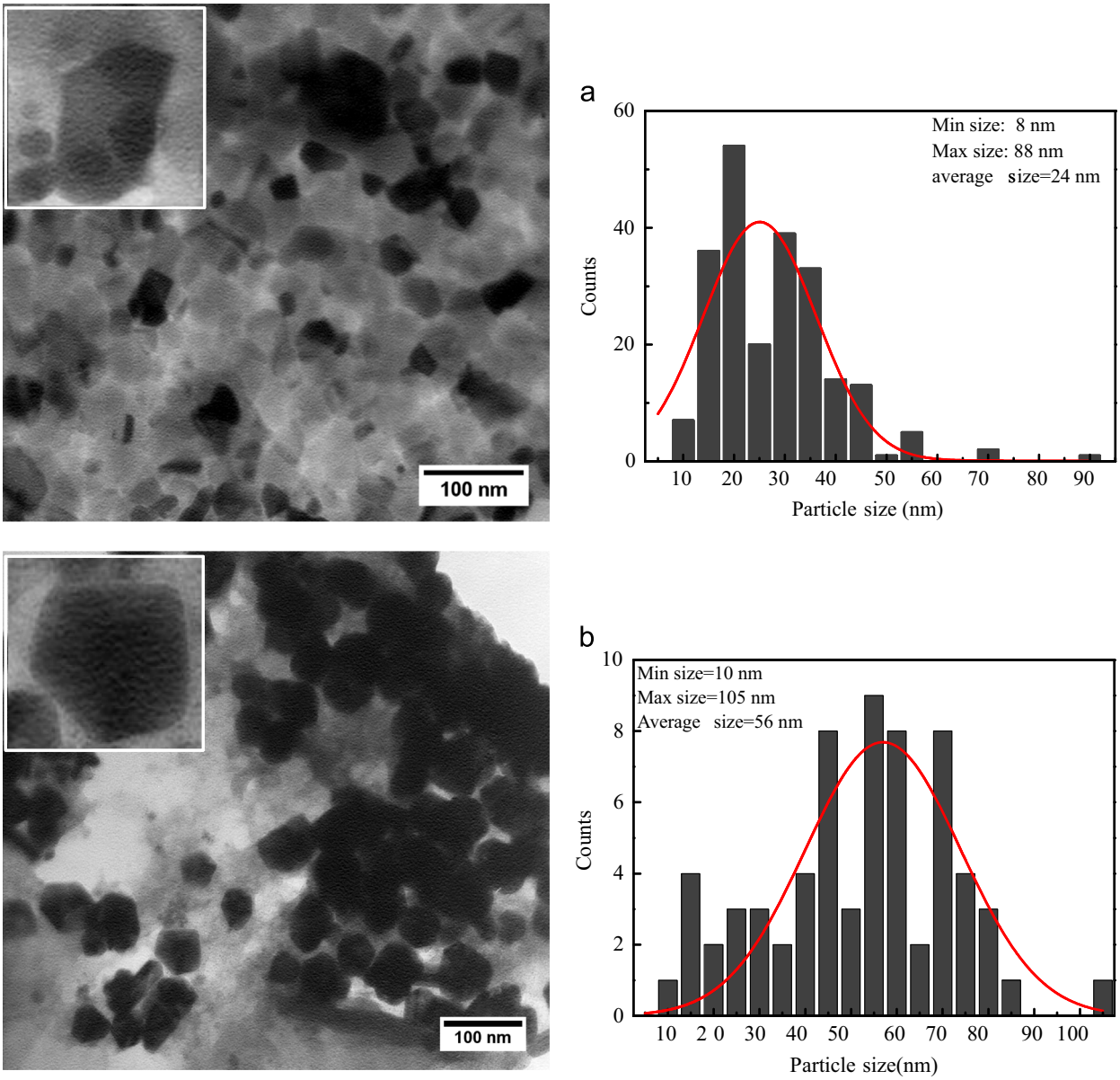

Fig. 2. Typical TEM images and corresponding size distribution histograms of (a) as-prepared blue colloidal sample and (b) after decolorization by $PdCl_2$ solution (sample $PM_{1:10}$).

other ones can be seen from behind. This shows that they are probably sheets in nature with thickness narrow enough for electrons to transmit through. This is possible because one of the most special characteristics of molybdenum oxide is its layered structure made of stacking up slabs (~0.7 nm thickness) of MoO_6 octahedrals [36]. Due to weak van der Waals internal forces between slabs, exfoliate of layered molybdenum trioxide gives discrete multilayer MoO_3 nanosheets in the presence of mechanical sonication and suitable solvent. It has been shown that the reduction in number of layers can increase the carries mobility of the material [37].

Size distribution histogram indicates that the as-prepared blue colloidal solution has a nearly uniform size distribution with about 24 nm average particles size. TEM image of sample $PM_{1:10}$ and corresponding size distribution histogram are shown in Fig. 2(b). Obviously, sample $PM_{1:10}$ consists of multifaceted nanoparticles and the average particle size has been increased to about 56 nm. Comparing these two images reveals that addition of palladium salt solution leads to increase of the colloidal particle size. However, it is not obvious how palladium salt causes this increase and whether it has been doped into the molybdenum oxide or not.

3.2. UV–vis spectroscopy of decolorization process

Optical absorption spectrum of as-prepared blue molybdenum oxide nanosheets (top curve in Fig. 3) displays an optical absorption band in the range of 1–3 eV. The rising magnitude of absorption above 3 eV is due to absorption across the optical band gap. One can recognize a major peak at 1.6 eV and three shoulders centered at photon energies of 1.2, 1.4, and 1.9 eV. After addition of $PdCl_2$ solution into blue samples, it was observed that the blue color gradually disappears. A sequential series of optical absorption spectra in different steps after adding $PdCl_2$ (sample $PM_{1:15}$) demonstrate time variation of spectra during the decolorization process. This decolorization was observed at all Pd:Mo ratio and depending on this ratio, it took a few minutes to several days for the primary blue nanosheets to transform to the colorless solution and elimination of the absorption peaks. Therefore, our results

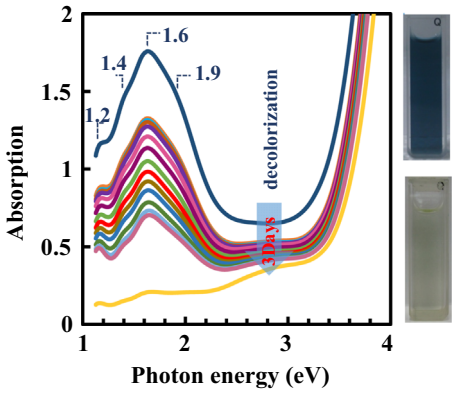

Fig. 3. Optical absorption spectra of as-prepared blue sample and recorded spectra during decolorization process of after addition of $PdCl_2$ solution with Pd:Mo=1:15. Right panel shows photograph images of as-prepared blue sample and after decolorization by $PdCl_2$ solution (sample $PM_{1:15}$). (For interpretation of the references to color in this figure legend, the reader is referred to the web version of this article.)

indicate that $PdCl_2$ is a decolorizing agent in addition to its catalytic role against hydrogen. To the best of our knowledge, no report has been given on this decolorization by $PdCl_2$ solution of blue molybdenum oxide so far.

3.3. X-ray photoelectron spectroscopy (XPS)

Generally, there is a strong relation between color of a metal oxide and oxidation states of its metal ions. On the other hand, XPS is a powerful tool for identification of oxidation states of metal oxides. Therefore, in order to investigate the variation of surface chemical composition of the blue molybdenum oxide nanoparticles upon decolorization process XPS was applied. Fig. 4(a) and (b) shows high-resolution XPS spectra of Mo3d core levels for the as-prepared blue sample and after decolorization by $PdCl_2$ (sample $PM_{1:10}$), respectively. The XPS spectrum of as-prepared sample consists of two Mo3d doublet with Mo3d5/2 binding energies at 232.8 and 231.7 eV, which are characteristic for molybdenum in 6+ and 5+ oxidation states, respectively [38]. It has been proven that Mo^{5+} state is responsible for the blue color in certain compositions of molybdenum oxide [36]. Decreasing trend in UV–vis absorption spectra before 3 days after addition of $PdCl_2$ clearly illustrates the decolorization procedure. Addition of $PdCl_2$ solution has a noticeable effect on molybdenum oxidation states. The Mo3d spectrum of sample $PM_{1:10}$ (Fig. 4(b)) shows two doublets involving one Mo3d5/2 peak at binding energy of 232.4 eV, the expected value of Mo^{6+} states, and one Mo^{5+} state with much less contribution at 230.9 eV. Therefore, addition of $PdCl_2$ leads to diminish of Mo^{5+} states. The changes in these two spectra can be interpreted by increase of the oxidation number from 5+ to 6+ in oxidation–reduction reaction of Mo with the Pd ions to form metallic palladium. High-resolution XPS spectrum of Pd3d in Pd–MO_3 sample is shown in Fig. 4(c). This spectrum could be fitted by two doublets one with higher intensity and one with much lower intensity. The major one has Pd3d5/2 and Pd3d3/2 peaks centered at 337.9 and 343.3 eV, respectively, which are in consistent with those reported for Pd^{2+} in $PdCl_2$ composition and the minor one has the corresponding peaks at 336.6 and 341.9 eV which are attributed to Pd^{2+} in PdO composition [39]. Therefore the $PdCl_2$ composition has been recovered again in the de-colorization process and led to appearance of Pd^{2+} states in XPS spectrum of Pd3d core level. According to these findings, we propose a reaction in which Mo^{5+} states covert to Mo^{6+} and Pd^{2+} reduces to Pd^0. Then Pd^0 provides electron for O_2 and H^+ to form H_2O. This reaction is shown schematically in Fig. 5. When all Mo^{5+}

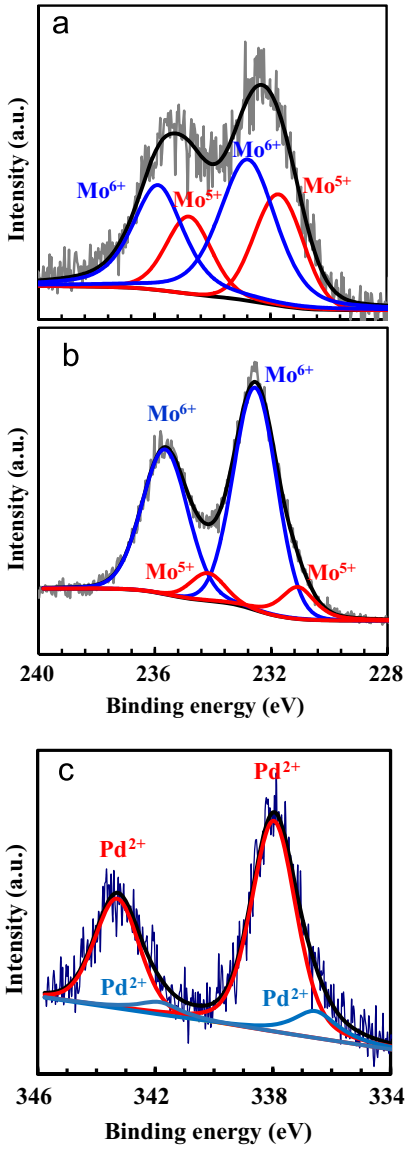

Fig. 4. High resolution XPS spectra of Mo3d core level for (a) as-prepared blue colloidal sample and (b) after decolorization by $PdCl_2$ (Pd:Mo=1:10) solution. (c) High resolution XPS spectrum of Pd3d in sample $PM_{1:10}$.

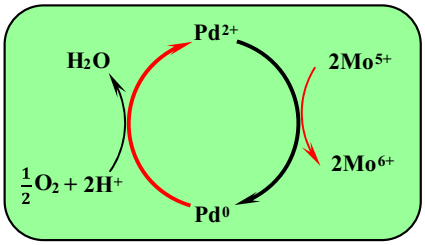

Fig. 5. Ping-pong mechanism of oxidation-reduction reaction in decolorization process of blue molybdenum oxide by $PdCl_2$ solution. Oxidation number of Mo^{5+} increases and Mo^{6+} are created.

are consumed by this ping-pong mechanism, the final product gives Pd^{2+} states which can be recovered in the drying process after reaction with Cl^- in the form of $PdCl_2$.

The XPS measurements of oxygen atoms in molybdenum oxide samples are shown in Fig. 6(a) and (b). For all the samples, the presence of two different O1s exhibits the possible O bonding such as in with molybdenum (lower binding energy) and hydrogen in

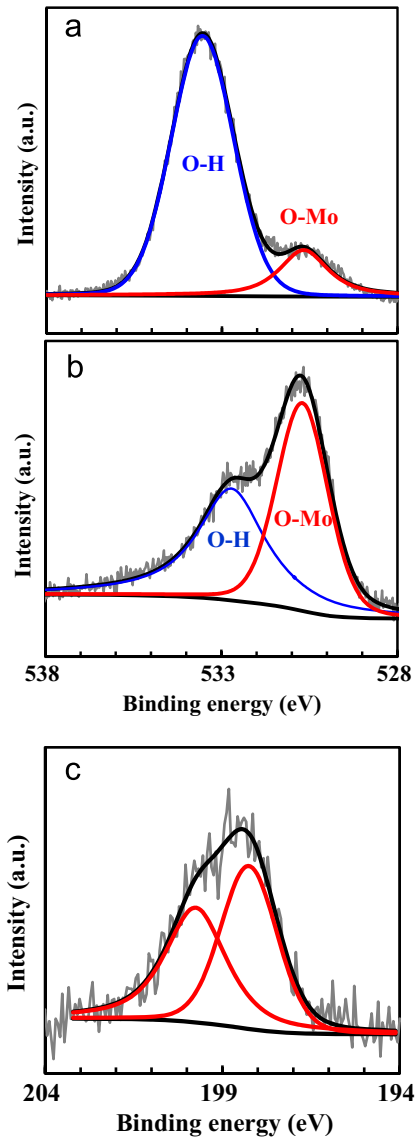

Fig. 6. High resolution XPS spectra of O1s core level for (a) as-prepared blue colloidal sample and (b) sample $PM_{1:10}$. (c) High resolution XPS spectrum of Cl2p in sample $PM_{1:10}$.

the form of hydroxyl groups (greater binding energy). The O1s spectrum of as-prepared sample differs much more from that of $PM_{1:10}$. For as-prepared sample, O_{1s} peak could be de-convoluted into two main peaks one at 530.7 eV and one broad intense peak at 533.6 eV. The first one is related to oxygen bonding with molybdenum atoms while those at 533.6 eV are related to O–H, O–C and/or oxygen absorbed contaminants species [40]. However, O1s XPS spectrum of sample $PM_{1:10}$ shows one peak located at higher binding energy (532.7 eV) with a reduced relative intensity. This observation confirms the suggestion that the water molecules could be desorbed from the structure in the process of the oxidation–reduction reaction. A room temperature mild and reversible method to convert amides to nitriles in good yields via dehydration process using $PdCl_2$ in aqueous media has been reported by Maffioli et. al [41]. The presence of strong O–H XPS peak in our as-prepared sample proposes that the as-prepared colloids are hydrate molybdenum oxide, hence it is expected that a mild dehydration process begins with adding $PdCl_2$ as well into the primary solution.

Using the peak area of O1s at lower binding energy (Mo–O bond) and all those of the Mo3d, the O/Mo ratio is estimated to be 2.5 in the as-prepared and 2.6 in the $PM_{1:10}$ samples. The presence of hydroxyl group in as-prepared sample with an intense peak probably originates from hydrate composition of colloidal nanoparticles. The hydroxyl peaks were also observed in the anodizing synthesis of tungsten oxide dihydrate in our previous work [18]. Addition of palladium salt has no considerable impact on the O:Mo ratio but greatly influences the presence of hydroxyl groups. For more evidence, the Cl2p region in the XPS spectrum of $PM_{1:10}$ sample is shown in Fig. 6(c). The Cl2p3/2 and Cl2p1/2 peaks that are centered at 198.4 and 200.1 eV and are related to the atomic chloride of $PdCl_2$ composition. The ratio of Cl:Pd is calculated to be 2.3. This is a value greater than the ratio in $PdCl_2$ composition, which is probably due to extra Cl from the 0.02 M HCl electrolyte.

3.4. Gasochromic properties

Despite few reports on gasochromic switching in molybdenum oxide films and that, most of which have not been reversible; our decolorized PM colloidal samples exhibited unique reversible in-liquid gasochromic coloration by hydrogen gas, which has not been reported before. The optical absorption spectra of PM samples with different Pd to Mo ratios were recorded step-by-step from the blue color (after gasochromic coloration by hydrogen bubbling) to the complete bleaching (by oxygen bubbling), which are shown in Fig.7(a)–(d). Inset of part (c) illustrates the photograph images the sample after 4 min hydrogen bubbling with 6 l/h flow rate. As can be seen, a strong gasochromic coloration occurs in the liquid phase in which the colorless sample converts to a homogenous dark blue color. This figure demonstrates the effect of Pd to Mo ratio on the shapes and time variations of optical absorption spectra in the gasochromic coloration process. The first point to be noted is that the maximum absorption peaks for all colored samples are observable once again at 1.6 eV, which is exactly equal to that of as-prepared blue samples. Moreover, almost for all the samples the previously observed shoulders in as-prepared blue samples can be found at the same points i.e. 1.2, 1.4 and 1.9 eV. However, there is a difference between as-prepared blue sample and gasochromic colored ones. The absorption spectra of gasochromic colored samples are about 0.6 eV wider than those of as-prepared sample. The absorption spectra of all kind of our blue samples starts to rise from 1.2 eV and drops to the background at about 2.4 eV for as-prepared blue sample (Fig. 3) while continues to about 3 eV for the gasochromic colored blue PM samples. For more interpretations, for all samples the absorption spectra were de-convoluted into five constructing peaks and one typical of this de-convolution for sample $PM_{1:15}$ is shown in Fig. 8(a). Hence for gasochromic coloration, there is an extra shoulder between 2–3 eV in the optical absorption spectra. We name this shoulder P5. In Fig. 8(b) the single peaks of P5 are plotted for different bleaching times. One can see that the behavior of P5 differs from peaks P1–P4 as it exhibits a red-shift (moving toward lower energies) over the bleaching process. Although peaks P1–P4 vary in intensity, their photon energy positions are almost fixed. Table 1 indicates the peak/shoulder positions at different bleaching times for sample $PM_{1:15}$. It shows that the peak position of P1–P4 are almost constant but shoulder P5 shifts by about 0.22 eV. This behavior could be observed for all the other samples. One can recognize that the maximum absorption increases with increase in the Pd:Mo ratio up to 1:15 and then reduces slightly at 1:20.

The as-prepared colloids which are blue in nature are permanently decolorized by adding PdCl2 without need to insertion of hydrogen. However, for re-coloring hydrogen is needed. So from this point of view Pd and $PdCl_2$ have same effects. However, if we focus on hydrogen diffusion and consider Pd or $PdCl_2$ as a catalyst for H_2 dissociation into protons, the subject falls into a diffusion process. Pd

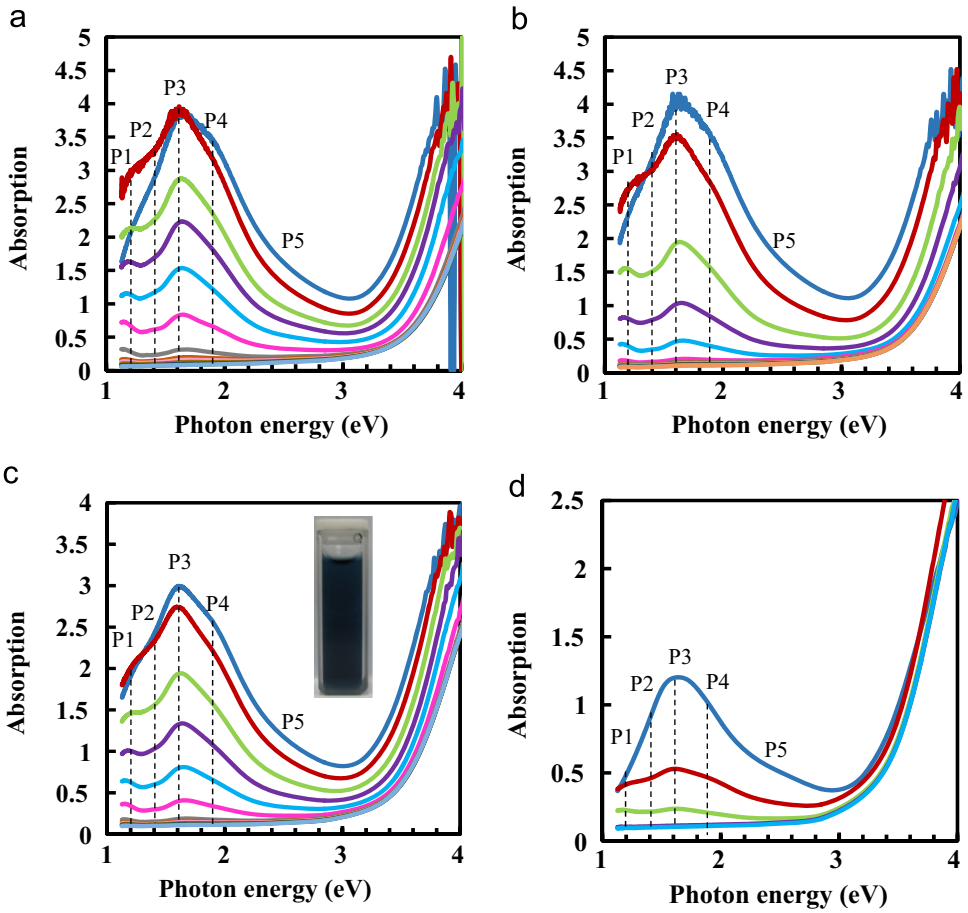

Fig. 7. Optical absorption spectra of PM samples with different Pd:Mo ratios during bleaching by oxygen bubbling after one gasochromic coloration process by hydrogen bubbling for 4 min. (a) $PM_{1:20}$, (b) $PM_{1:15}$, (c) $PM_{1:10}$ and (d) $PM_{1:5}$. The inset of part (c) shows corresponding photograph image after gasochromic coloration by diluted hydrogen bubbling.

or $PdCl_2$ has nearly the same role: they assist proton transfer from a high to a low hydrogen chemical potential. Based on this thought, the initial blue samples involve hydrogen in the lattice and $PdCl_2$ or Pd is a catalyst for diffusing them into the ambient condition (hydrogen free). So decolorization happens. But when hydrogen is bubbled the diffusion direction reverse and coloring happens. However, there remains a question yet; why an extra optical absorption shoulder appears for hydrogen coloring. This is not clear for us right now, but it may be related to different lattice positions of H between primary and new inserted hydrogens.

Since palladium content can control the proton formation rate from dissociation of hydrogen, increase of palladium leads to increase in the optical absorption within the gasochromic process. On the other hand, probably excess palladium limits the hydrogen intercalation level because of trapping of hydrogen atoms in palladium. Extra palladium is deal with larger palladium clusters with reduced chemical activity due to lower surface/volume ratio. Hydrogen feed for MoO*x* nanoparticles is supposed to do by spillover mechanism in which saturated hydrogens spills over across the Pd surfaces. It is expected that smaller particle saturated faster and provide higher hydrogen feed. It can also be attributed partially to the formation of PdH_x phase with less optical absorption.

Up to now, there is no unique model to satisfactory describe the optical absorption in gasochromic coloring effect when hydrogen atoms are inserted into molybdenum oxide structure. The papers on chromic thin films in literature propose different models including three band absorption [42], small polaron transition [22,23], double injection mechanism [24] and a new model of oxygen vacancies [1]. Indeed, the small polaron theory describing the coloring effect in tungsten oxide films predicts that the polaron energies, hence the absorption peak positions, vary with color center concentration which is proportional to the optical density. In a review articles by Deb [43], it has been reflected that the coloration in amorphous WO_3 is due to small polaron formation. In that case, the small polaron binding energy ($-E_p$) is given by the relation:

$$-E_p = \frac{1}{2}\frac{e^2}{r_p}\left(\frac{1}{\varepsilon_\alpha} - \frac{1}{\varepsilon_0}\right) \quad (1)$$

where ε_α and ε_0 are optical and static dielectric constants, respectively, and r_p (polaron radius) is given by

$$r_p = \frac{1}{2}\sqrt[3]{\pi/6N_p} \quad (2)$$

where N_p is the polaron number density per unit volume. This suggests that as N_p increases, E_p also increases, which supports the observation that the color center peak moves to higher energy with increasing coloration density. Accordingly, the extra shoulder and the observed red-shift in gasochromic coloration of our colloidal molybdenum oxide can be described on the basis of small polaron concept. Then this question is arises what is the origin of P1–P4 peaks?. Although the answer is not completely clear for us right now, we try to check the satisfactory of the observed peaks based on the presents models; intervalence charge transfer (IVCT), d-d transition and interband charge transfer. In a work by Dieterle

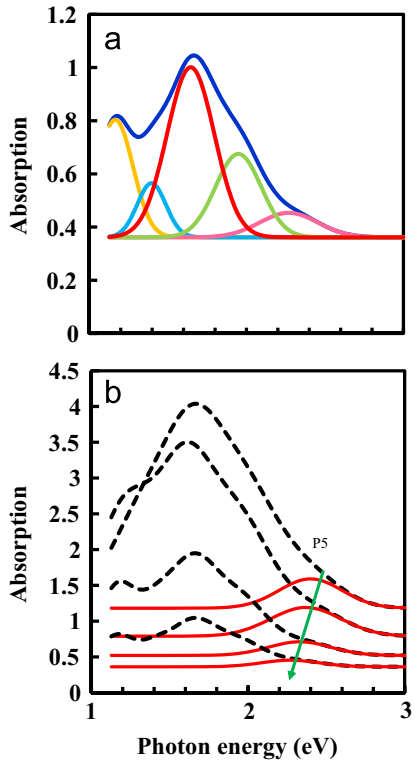

Fig. 8. (a) De-convolution of a typical absorption spectrum into different constructing peaks and (b) variation of peak P5 in the bleaching process for sample $PM_{1:15}$.

Table 1
peak position of sample $PM_{1:15}$ in the bleaching process (see Fig. 7(c)).

spectrum	Peak position (eV)				
	P1	P2	P3	P4	P5
1	1.25	1.41	1.63	1.95	2.39
2	1.19	1.42	1.66	1.93	2.36
3	1.13	1.38	1.63	1.91	2.31
4	1.16	1.39	1.64	1.94	2.26
5	1.14	1.39	1.65	1.94	2.17

et. al [44] absorption bands at 2.03 and 1.28 eV were assigned to IVCT transition of type Mo^{5+}–O–Mo^{6+} → Mo^{6+}–O–Mo^{5+}. The absorption band at 2.03 was attributed to an oxygen vacancy defect state like [$Mo^{5+}O_5$], while the band at 1.28 was attributed to an IVCT transition of a hexacoordinated defect like [$Mo^{5+}O_6$]. So in the first model framework P1 (1.2 eV) and P4 (1.9 eV) in our work can be attributed to such IVCT transition. According to Dieterle, when comparing the energetic positions of the [$Mo^{5+}O_5$] and the [Mo5+O6] defect states within the bandgap, the higher symmetry of the [$Mo^{5+}O_6$] defect leads to an energetically more favorable state due to a better charge compensation than the lower symmetry of [$Mo^{5+}O_5$] and this is why the peak P1 is stronger than peak P4 (Fig. 8(a)). The peak positions near those of our P2 and P5 have been attributed to Mo^{5+}–O^{2-} ligand to metal charge transfer (LMCT) and Mo^{5+} d-d transitions of a heavily distorted polyhedron in an octahedral crystal field. Peak at 1.6 eV originates from d-d transition in [$Mo^{5+}O_6$] octahedron and 2.4 eV from [$Mo^{5+}O_5$] pentahedron. One can see again that the intensity of peak P2 (2.4 eV) is stronger than P5 (2.4 eV). We attribute the peak P3 (1.4 eV) to the d-d transition possibly one same as P2. In addition to d-d transitions the possible LMCT can be originated from different types of reactions within which charges are transferred. For example one can consider the following transitions:

$$O^{2-} + Mo^{6+} \rightarrow O^{-} + Mo^{5+}$$

$$O^{-} + Mo^{5+} \rightarrow O^{-} + Mo^{4+}$$

$$(OH)^{-} + Mo^{6+} \rightarrow (OH)^{0} + Mo^{5+}$$

$$(OH)^{-} + Mo^{5+} \rightarrow (OH)^{0} + Mo^{4+} \quad (3)$$

In a work by Schirmer et. al the formation of peak between 1–1.5 eV in crystalline H_xWO_3 composition was attributed to formation of bipolaron from the creating of W^{5+} states [45]. According to bipolaron model, conduction electrons in low temperature phase of crystalline WO_{3-x} ($x > 0.0001$) are diamagnetically paired and forming bipolarons due to joint lattice deformation. They can be dissociated with light in a broad band of wavelengths peaks at 1.1 eV which is monitored by appearance of W^{5+} states and corresponding change in DC electrical conductivity.

In another interpretation we note on the optical band gap of colorless $PM_{1:15}$ samples calculated by Tauc formula (not shown here) which gives value of 3.0 eV. On the other hand, the peak energy sum of pair P1 (1.2)–P4 (1.9) and those of pair P2 (1.4)–P3 (1.6) are very close to 3 i.e. the band gap value. This fact suggests a simple model in which two different inter-band states are forming between valence and conduction band with 1.6 and 1.2 for example above the valence band as the colloidal samples are colored by hydrogen (Fig. 9). These states may be in relation to lower oxidation states of molybdenum namely Mo^{5+}. According to the above finding, one can assert that the gasochromic coloration phenomena in metal oxides like MoO_3 or WO_3 do not deal with only one unique mechanism. But instead, formation of small polarons which describe electron–phonon coupling and formation of inter-band states which is an electronic point of view are possible at the same time. Comparing with gasochromic tungsten oxide colloids in our previous work, in the case of MoO_3 colloids peak P2 is dominant in the whole duration of coloring bleaching process, while for WO_3 there was Bactrian camel hump-like peaks at deep color states which are converted to Dromedary camel hump-like peaks with bleaching.

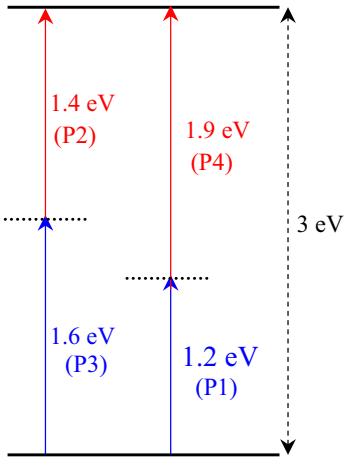

Fig. 9. Schematic representation of the proposed inter-band transition model for the coloration mechanism in the molybdenum oxide colloidal solutions.

4. Conclusion

Anodizing of Mo sheets in dilute HCl electrolyte have been used for synthesis of blue molybdenum oxide nanoparticles as a gasochromic colloidal solution. The palladium chloride was found to be a decolorization agent by which, the blue colloids convert to a colorless colloidal solution. The oxidation state of molybdenum in blue solution is a mixture of Mo^{5+} and Mo^{6+} while in decolorized one the oxidation number increases. It was found also that initial nanoparticles have probably water in their structure which can be removed by palladium chloride. This compound can be served as a liquid gasochromic system because hydrogen bubbling caused the decolorized solution colored again. The initial blue samples represented optical absorption bands in NIR region in which different shoulders could be recognized. The gasochromic colored sample showed an extra shoulder in addition to those of initial samples which undergoes a red-shift up on bleaching in oxygen. The observed shift was attributed to the mechanism of small polaron transition and the other peaks were almost fixed in their position and were explained by inter-band transition model.

References

[1] V. Wittwer, M. Datz, J. Ell, A. Georg, W. Graf, G. Walze, Gasochromic windows, Sol. Energy Mater. Sol. Cells 84 (2004) 305–314.
[2] A. Georg, W. Graf, R. Neumann, V. Wittwer, Mechanism of the gasochromic coloration of porous WO_3 films, Solid State Ion. 127 (2000) 319–328.
[3] S.K. Deb, Opportunities and challenges in science and technology of WO_3 for electrochromic and related applications, Sol. Energy Mater. Sol. Cells 92 (2008) 245–258.
[4] R. Baetens, B.P. Jelle, A. Gustavsen, Properties, requirements and possibilities of smart windows for dynamic daylight and solar energy control in buildings: a state-of-the-art review, Sol. Energy Mater. Solar Cells 94 (2010) 87–105.
[5] J.L. Slack, J.C.W. Locke, S.W. Song, J. Ona, T.J. Richardson, Metal hydride switchable mirrors: factors influencing dynamic range and stability, Sol. Energy Mater. Solar Cells 90 (2006) 485–490.
[6] M. Slaman, B. Dam, H. Schreuders, R. Griessen, Optimization of Mg-based fiber optic hydrogen detectors by alloying the catalyst, Int. J. Hydrog. Energy 33 (2008) 1084–1089.
[7] W.C. Hsu, C.C. Chan, C.H. Peng, C.C. Chang, Hydrogen sensing characteristics of an electrodeposited WO_3 thin film gasochromic sensor activated by Pt catalyst, Thin Solid Films 516 (2007) 407–411.
[8] C.C. Chan, W.C. Hsu, C.C. Chang, C.S. Hsu, Preparation and characterization of gasochromic Pt/WO_3 hydrogen sensor by using the Taguchi design method, Sens. Actuators, B: Chem 145 (2010) 691–697.
[9] S.S. Kalanur, Y.A. Lee, H. Seo, Eye-readable gasochromic and optical hydrogen gas sensor based on CuS–Pd, RSC Adv. 5 (2015) 9028–9034.
[10] L. Berggren, A. Azens, G.A. Niklasson, Polaron absorption in amorphous tungsten oxide films, J. Appl. Phys. 90 (2001) 1860–1863.
[11] G.A. Niklasson, J. Klasson, E. Olsson, Polaron absorption in tungsten oxide nanoparticle aggregates, Electrochim. Acta 46 (2001) 1967–1971.
[12] G.A. Niklasson, C.G. Granqvist, Electrochromics for smart windows: thin films of tungsten oxide and nickel oxide, and devices based on these, J. Mater. Chem. 17 (2007) 127–156.
[13] H. Takeda, K. Adachi, Near infrared absorption of tungsten oxide nanoparticle dispersions, J. Am. Ceram. Soc. 90 (2007) 4059–4061.
[14] G.A. Niklasson, L. Berggren, A.-L. Larsson, Electrochromic tungsten oxide: the role of defects, Sol. Energy Mater. Sol. Cells 84 (2004) 315–328.
[15] R. Zacharia, K.Y. Kim, A.K.M. Fazle Kibria, K.S. Nahm, Enhancement of hydrogen storage capacity of carbon nanotubes via spill-over from vanadium and palladium nanoparticles, Chem. Phys. Lett. 412 (2005) 369–375.
[16] A.C.C. Tseung, K.Y. Chen, Hydrogen spill-over effect on Pt/WO_3 anode catalysts, Catal. Today 38 (1997) 439–443.
[17] M. Ranjbar, H. Kalhori, S. Mahdavi, New gasochromic system: nanoparticles in liquid, J. Nanopart. Res. 14 (2012) 1–10.
[18] M. Ranjbar, A.H. Fini, H. Kalhori, P. Kameli, H. Salamati, , Gasochromic effect in colloidal nanoparticles of tungsten oxide dihydrate synthesized via a simple anodizing method, Sol. Energy Mater. Sol. Cells 132 (2015) 329–336.
[19] J. Okumu, F. Koerfer, C. Salinga, M. Wuttig, In situ measurements of thickness changes and mechanical stress upon gasochromic switching of thin MoO*x* films, J. Appl. Phys. 95 (2004) 7632–7636.
[20] M.H. Yaacob, J. Yu, K. Latham, K. Kalantar-Zadeh, W. Wlodarski, Optical hydrogen sensing properties of nanostructured Pd/MoO_3 films, Sens. Lett. 9 (2011) 16–20.
[21] Z. Zhang, G. Wu, G. Gao, W. Feng, X. Jin, J. Shen, Structural study of WO_3 and MoO_3 compound films in H_2 gasochromism, Key Eng. Mater. 537 (2013) 184–188.
[22] A. Prasad, D. Kubinski, P. Gouma, Comparison of sol–gel and ion beam deposited MoO_3 thin film gas sensors for selective ammonia detection, Sens. Actuators B: Chem. 93 (2003) 25–30.
[23] S. Sunu, E. Prabhu, V. Jayaraman, K. Gnanasekar, T. Seshagiri, T. Gnanasekaran, Electrical conductivity and gas sensing properties of MoO_3, Sens. Actuators B: Chem. 101 (2004) 161–174.
[24] Y. Li, Y. Bando, D. Golberg, K. Kurashima, Field emission from MoO_3 nanobelts, Appl. Phys. Lett. 81 (2002) 5048–5050.
[25] L. Campanella, G. Pistoia, MOO_3: a new electrode material for nonaqueous secondary battery applications, J. Electrochem. Soc. 118 (1971) 1905–1908.
[26] L. Zhou, L. Yang, P. Yuan, J. Zou, Y. Wu, C. Yu, α-MoO_3 nanobelts: a high performance cathode material for lithium ion batteries, J. Phys. Chem. C 114 (2010) 21868–21872.
[27] N.A. Chernova, M. Roppolo, A.C. Dillon, M.S. Whittingham, Layered vanadium and molybdenum oxides: batteries and electrochromics, J. Mater. Chem. 19 (2009) 2526–2552.
[28] J. Yao, K. Hashimoto, A. Fujishima, Photochromism induced in an electrolytically pretreated MoO_3 thin film by visible light, Nature 355 (1992) 624–626.
[29] N. Mcevoy, J.N. Coleman, G.S. Duesberg, V. Nicolosi, Production of molybdenum trioxide nanosheets by liquid exfoliation and their application in high-performance supercapacitors, 2014.
[30] D. Mariotti, H. Lindström, A.C. Bose, K.K. Ostrikov, Monoclinic β-MoO_3 nanosheets produced by atmospheric microplasma: application to lithium-ion batteries, Nanotechnology 19 (2008) 495302.
[31] L. Zhang, Y. Tu, J.H. Cui, W.C. Shi, Q. Li, Synthesis and photo-catalytic properties of MoO_3 nanosheets, Key Eng. Mater. 602 (2014) 42–45.
[32] J. Yang, F. Lu, Y. Li, S. Yang, R. Li, N. Huo, C. Fan, Z. Wei, J. Li, S.-S. Li, Low temperature electrical transport and photoresponsive properties of H-doped MoO_3 nanosheets, J. Mater. Chem. C 2 (2014) 1034–1040.
[33] G. Ali, H.J. Kim, J.M. Kum, S.O. Cho, Rapid synthesis of TiO_2 nanoparticles by electrochemical anodization of a Ti wire, Nanotechnology 24 (2013) 185601–185608.
[34] Y. Tang, D. Gong, Y. Lai, Y. Shen, Y. Zhang, Y. Huang, J. Tao, C. Lin, Z. Dong, Z. Chen, Hierarchical layered titanate microspherulite: formation by electrochemical spark discharge spallation and application in aqueous pollutant treatment, J. Mater. Chem. 20 (2010) 10169–10178.
[35] L. Zheng, Y. Xu, D. Jin, Y. Xie, Novel metastable hexagonal MoO_3 nanobelts: synthesis, photochromic, and electrochromic properties, Chem. Mater. 21 (2009) 5681–5690.
[36] Q. Huang, S. Hu, J. Zhuang, X. Wang, MoO_{3-x}-based hybrids with tunable localized surface plasmon resonances: chemical oxidation driving transformation from ultrathin nanosheets to nanotubes, Chem.– Eur. J. 18 (2012) 15283–15287.
[37] D.D. Yao, J.Z. Ou, K. Latham, S. Zhuiykov, A.P. O'Mullane, K. Kalantar-zadeh, Electrodeposited α-and β-phase MoO_3 films and investigation of their gasochromic properties, Cryst. Growth Des. 12 (2012) 1865–1870.
[38] J.G. Choi, L.T. Thompson, XPS study of as-prepared and reduced molybdenum oxides, Appl. Surf. Sci. 93 (1996) 143–149.
[39] M. Ranjbar, S. Fardindoost, S. Mahdavi, N. Tahmasebi, Palladium nanoparticle deposition onto the WO_3 surface through hydrogen reduction of $PdCl_2$: characterization and gasochromic properties, Sol. Energy Mater. Sol. Cells 95 (2011) 2335–2340.
[40] J. Kukkola, J. Mäklin, N. Halonen, T. Kyllönen, G. Tóth, M. Szabó, A. Shchukarev, J.P. Mikkola, H. Jantunen, K. Kordás, Gas sensors based on anodic tungsten oxide, Sens. Actuators B: Chem. 153 (2011) 293–300.
[41] S.I. Maffioli, E. Marzorati, A. Marazzi, Mild and reversible dehydration of primary amides with $PdCl_2$ in aqueous acetonitrile, Org. Lett. 7 (2005) 5237–5239.
[42] U. Tritthart, W. Gey, A. Gavrilyuk, Low temperature coloration of WO_3 and MoO_3 thin films, Ionics 4 (1998) 299–308.
[43] S.K. Deb, Opportunities and challenges of electrochromic phenomena in transition metal oxides, Sol. Energy Mater. Sol. Cells 25 (1992) 327–338.
[44] M. Dieterle, G. Weinberg, G. Mestl, Raman spectroscopy of molybdenum oxides Part I. Structural characterization of oxygen defects in MoO_{3-x} by DR UV/vis, Raman spectroscopy and X-ray diffraction, Phys. Chem. Chem. Phys. 4 (2002) 812–821.
[45] O.F. Schirmer, E. Salje, Conduction bipolarons in low-temperature crystalline WO $_{3-x}$, J. Phys. C: Solid State Phys. 13 (1980) L1067.